On the orientation and absolute phase of marine CSEM receivers

Rune Mittet[1], Odd Marius Aakervik[1], Hans Roger Jensen[1], Svein Ellingsrud[1], and Alexey Stovas[2]

ABSTRACT

Receiver orientation can be recovered from electric and/or magnetic data if it is not directly measured. A receiver dropped on the seabed will end up with an arbitrary orientation, which means that the recorded electric and magnetic x- and y-components will point in arbitrary directions. We demonstrate how both electric and magnetic data can be used to rotate the field data to a coordinate system where the x-direction points in the inline or towline direction or $180°$ with respect to this direction. The amplitudes of electric and magnetic marine CSEM data are highly offset dependent so we introduce a median filtering approach to handle this problem. An inspection of the electric and/or magnetic phase after normalization with the source-current phase can resolve the remaining problem of the 180 degree spatial rotation. The result is electric and magnetic data where the x-component points in the positive towline direction. We analyze the case of lost temporal synchronization between receivers and the transmitter and show that the proper absolute phase can be recovered approximately by producing precalculated tables for zero or minimum offset of the electric and/or magnetic phase. These tables depend on the frequency, the transmitter length, the water conductivity, and the distance between the receiver and the midpoint of the transmitter. These four quantities are measured during a marine CSEM survey. The method requires electric and/or magnetic data that are not saturated at short offsets. The magnetic zero or minimum offset phase shows less variation with these four parameters than the electric zero or minimum offset phase. Hence, if magnetic data are available, they are preferable to electric data for this type of processing.

INTRODUCTION

Marine controlled-source electromagnetics (CSEM) as originally suggested by Cox et al. (1971) and Young and Cox (1981), and was later followed by contributions from Constable (1990), Constable and Cox (1996), Yuan and Edwards (2000), and MacGregor et al. (2001). These were nonhydrocarbon-related studies except for Yuan and Edwards (2000) who investigated marine gas hydrates. The application of this method to hydrocarbon exploration, also named seabed logging (SBL), is described by Eidesmo et al. (2002) and Ellingsrud et al. (2002). The main idea is to use an active source to probe the underground for thin, highly resistive layers. Hydrocarbon-filled reservoirs typically have a resistivity that is one to two orders of magnitude higher than a water-filled reservoir and the surrounding shale or mudrock. This is sufficient to support a channeled field in the reservoir which will leak energy up to receivers placed on the seabed. The SBL experiment consists of dropping electric and magnetic sensors onto the seabed along a predetermined sail line and subsequently towing a horizontal electric dipole source along this line. The sail line starts approximately 10 km before the first receiver and ends approximately 10 km after the last receiver. Thus, all receivers have active source data with source receiver offsets of 10 km. The receivers will spin around the vertical axis on the way from the sea surface to the seabed and have an arbitrary orientation when they reach the seabed.

The measurement of the receiver orientation can be performed by a gyroscope, but there are at least two reasons why this is not a standard solution. A sufficiently accurate gyroscope has a relatively high cost and is also energy consuming. Solving the last problem requires larger battery packages and increases the weight of the receivers which is an unwanted side effect. Compasses are another possible solution for orientation measurements. They are standard equipment on all receivers, but they have accuracy problems. Compasses must be carefully calibrated when placed on a receiver. For example, if the battery package is changed, then the compass must be recalibrated. This means a recalibration of the compass each time a receiver is

dropped. This is not a trivial procedure on board the survey vessel. Thus the receiver orientation may not be sufficiently well determined if the receivers have only compass measurements. The first part of this paper discusses how receiver orientation can be determined approximately in a preprocessing step for certain experimental configurations. There is still a ±180° ambiguity in true receiver orientation after this first step. We solve this ambiguity by analyzing the phase behavior of the electromagnetic nearfield. Key (2003) studied the same type of 180° ambiguity for magnetotalluric (MT) data. With such data, a solution is to require the positivity of the diagonal elements of the transfer tensor.

Towing the transmitter over a resistive body versus a conductive body, one of the characteristic responses of the resistive layer is increased amplitude in the measured electric field. Data from a receiver with a towline over a generally conductive formation can be chosen as a reference. An anomaly can be identified by normalizing the amplitude for each receiver using the reference data set. Relative amplitudes that are large compared to unity may indicate a resistive body in the subsurface. However, the depth of the resistive body cannot be found with this qualitative technique. The depth to a resistive body can be found either by depth migration or inversion techniques. Depth migration techniques require an absolute phase in order to position a resistive body at the correct depth. Absolute phase also improves the depth constraint for inverse schemes. Measuring the absolute phase requires accurate time measurements and in particular that the clock timestamping the transmitter current is synchronized with the clock timestamping the receiver data.

There is information in the combined measurement of the transmitter current and receiver data that makes it possible to control the quality of this synchronization. Alternatively, if for some reason synchronization is lost, there may be sufficient information in the data to recover synchronization if the navigation is sufficiently accurate.

The method proposed here is based on analyzing the phase of the electric and/or magnetic field at the minimum transmitter/receiver separation. This analysis requires electric and magnetic data that are not saturated at small offsets. Saturation is a problem for most receiver systems in use today. This is due to the large dynamic range of the electric and magnetic fields over a distance from zero offset up to an offset of 10–15 km. EMGS uses automatic gain control (AGC) together with a 24-bit analog-to-digital converter (ADC) in the amplifiers to avoid the saturation of signals. The amplifier/ADC system then achieves a dynamic range which is larger than 200 dB. The AGC software measures the signal amplitude continuously within a given period. Depending on the signal level during this period, the next gain level is calculated. If the signal increases very quickly, the gain level will be immediately forced to a lower level to avoid any form of saturation.

SPATIAL ROTATION

The two horizontal electric components measured in the receivers local coordinate system are denoted $e_x(x_r|x_s,\omega)$ and $e_y(x_r|x_s,\omega)$, where x_r is the receiver position, x_s is the source position, and ω is angular frequency. We choose the towline direction to be our desired x-direction. This will also be referred to as the inline direction. The receivers are dropped to the seabed and, in general, the x-direction of the receiver will not coincide with the towline direction. However, the measured components can be rotated so that the new x-direction coincides with the towling direction. The two horizontal electric components in the coordinate system where the x-direction coin-

cides with the towline direction are $E_x(x_r|x_s,\omega)$ and $E_y(x_r|x_s,\omega)$. Thus,

$$E_x(x_r|x_s,\omega) = e_x(x_r|x_s,\omega)\cos(\theta) - e_y(x_r|x_s,\omega)\sin(\theta),$$
$$E_y(x_r|x_s,\omega) = e_x(x_r|x_s,\omega)\sin(\theta) + e_y(x_r|x_s,\omega)\cos(\theta), \quad (1)$$

and,

$$e_x(x_r|x_s,\omega) = E_x(x_r|x_s,\omega)\cos(\theta) + E_y(x_r|x_s,\omega)\sin(\theta),$$
$$e_y(x_r|x_s,\omega) = -E_x(x_r|x_s,\omega)\sin(\theta) + E_y(x_r|x_s,\omega)\cos(\theta). \quad (2)$$

We assume a right-handed coordinate system with the depth axis pointing downward. The orientation angle θ is measured positive in a clockwise direction and relative to the towline direction. Let us assume that the towline direction is from west to east. The desired coordinate system then has the positive x-axis to the east and the positive y-axis to the south. If the receiver arrives at the seabed with the receiver x-axis pointing east, then $\theta = 0$, and no rotation is required. For a receiver that arrives at the seabed with the receiver x-axis pointing south $\theta = \pi/2$. The receiver y-axis is pointing in the negative towline direction, which is also the negative x-direction in the desired coordinate system. Thus, the inline electric field is measured as the receiver $e_y(x_r|x_s,\omega)$ component, but with the wrong sign. We see that by applying equation 1 with $\theta = \pi/2$, the receiver $e_y(x_r|x_s,\omega)$ component is rotated into the $E_x(x_r|x_s,\omega)$ component with a desired sign reversal.

Ideally the orientation angle should be measured, but an approximation can be found from the data if it is not measured directly. We propose to use a least-squares method to find the orientation angle. The optimization criterion is based on symmetry considerations. The crossline electric field should be at a minimum when the transmitter points in the towline or inline direction. Thus, we seek a minimum in the crossline electric field,

$$E_y(x_r|x_s;\omega) = e_x(x_r|x_s,\omega)\sin(\theta) + e_y(x_r|x_s,\omega)\cos(\theta). \quad (3)$$

The approximation is good if the transmitter points in the direction of the towline and the earth locally is well described by plane layer geometry. In this case the electric field normal to the towline direction should be zero, but we never see this in real data even for optimal experimental conditions. In real data we have both additive (random) noise and multiplicative noise. Part of the multiplicative noise can be transmitter generated, in which case there are noise contributions with the same offset behavior as the electric and magnetic fields. These noise contributions will not be removed by performing a coordinate transform, but will be present in the crossline electric field after inline rotation. For real data and under good experimental conditions, we find that after inline rotation, the crossline amplitude is approximately 1%–3% of the inline electric field amplitude at intermediate and large offsets. Our experience is that after inline rotation, the ratio of the crossline electric field to the inline electric field is generally larger at small offsets. The reason may be that the relative contribution from noise is somewhat higher at small offsets. This is why we prefer to use intermediate and large offsets (2–10 km) for determining rotation angles. An alternative to seeking a minimum in E_y is to seek a minimum of the inline magnetic component H_x for the same experimental configuration. This component should be at a minimum if the transmitter points in the towline direction and the plane layer assumption is reasonable. The derivation to follow is for the electric field. The derivation for the magnetic field is then trivial.

In order to determine the rotation angle θ, we minimize the least squares expression,

$$\varepsilon_E = \sum_{x_s} \sum_{\omega} W(x_r|x_s,\omega)E_y(x_r|x_s,\omega)E_y^*(x_r|x_s,\omega), \quad (4)$$

or with $E_y(x_r|x_s,\omega)$ in terms of the measured (receiver) field components,

$$\varepsilon_E = \sum_{x_s} \sum_{\omega} W(x_r|x_s,\omega)(e_x(x_r|x_s,\omega)\sin(\theta)$$
$$+ e_y(x_r|x_s,\omega)\cos(\theta))(e_x(x_r|x_s,\omega)\sin(\theta)$$
$$+ e_y(x_r|x_s,\omega)\cos(\theta))^*. \quad (5)$$

$W(x_r|x_s,\omega)$ is a weighting function that compensates for the strong offset dependence of the electric field amplitude. We have tried several weighting schemes for equation 5. One possible choice is as in Mittet et al. (2004), where $W(x_r|x_s,\omega)$ is generated from inline synthetic data. $W(x_r|x_s,\omega)$ is then inversely proportional to the squared value of the inline synthetic electric field. Our implementation of this method gives the best results using intermediate and large offsets, so a minimum offset of 2 km is used. This weighting scheme equalizes the amplitude of the kernel of ε_E as a function of source-receiver offset.

The proposed method is reasonably robust with respect to the resistivity model used to generate the weighting function, however, it is sensitive to noise spikes in the data. Consequently, we have now changed to a weighting scheme of a different type and use a median filtering approach. Here, the weighting function is defined as a box-car function with zeros everywhere except for some offset interval, which is typically 250–500 m in length. Over this interval the offset dependence in the data is reasonably small, so the weights are set to unity. This removes the need for synthetic data to generate weighting functions. For this scheme we can use shorter offsets than 2 km for high quality data.

As an example of the filtering procedure, first we calculate a rotation angle using a weighting function that mutes all data except offsets from 2000 m to 2400 m. Next we calculate a rotation angle using a weighting function that mutes all data except offsets from 2400 to 2800 m. The procedure is continued up to the maximum offset which usually is 10,000 m. Finally, the rotation angle is determined by median filtering of the set of obtained rotation angles.

To simplify the formalism we define the partial sums,

$$\Gamma_{xx} = \sum_{x_s} \sum_{\omega} W(x_r|x_s,\omega)e_x(x_r|x_s,\omega)e_x^*(x_r|x_s,\omega),$$

$$\Gamma_{xy} = \sum_{x_s} \sum_{\omega} W(x_r|x_s,\omega)\frac{1}{2}(e_x(x_r|x_s,\omega)e_y^*(x_r|x_s,\omega)$$
$$+ e_x^*(x_r|x_s,\omega)e_y(x_r|x_s,\omega)),$$

$$\Gamma_{yy} = \sum_{x_s} \sum_{\omega} W(x_r|x_s,\omega)e_y(x_r|x_s,\omega)e_y^*(x_r|x_s,\omega). \quad (6)$$

Equation 5 is then expressed as,

$$\varepsilon_E = \Gamma_{xx}\sin^2(\theta) + 2\Gamma_{xy}\sin(\theta)\cos(\theta) + \Gamma_{yy}\cos^2(\theta). \quad (7)$$

An extremum requires $\partial_\theta \varepsilon_E = 0$ and this extremum being a minimum requires $\partial_\theta^2 \varepsilon_\varepsilon > 0$.

The rotation angle that minimizes $E_y(x_r|x_s,\omega)$ is then given by,

$$\tan(2\theta) = \frac{-2\Gamma_{xy}}{\Gamma_{xx} - \Gamma_{yy}}, \quad (8)$$

in the case of a positive second derivative, that is if,

$$(\Gamma_{xx} - \Gamma_{yy})\cos(2\theta) - 2\Gamma_{xy}\sin(2\theta) > 0. \quad (9)$$

If the second derivative is negative, then we are at a maximum for $E_y(x_r|x_s,\omega)$ and the minimum is at $\theta = \pm\pi/2$, if θ is measured in radians or $\theta = \pm90$, if θ is measured in degrees. Whether to use a plus or minus sign does not matter because the prescribed method minimizes $E_y(x_r|x_s,\omega)$. There are two possible solutions to a minimum in $E_y(x_r|x_s,\omega)$. The desired solution is when $E_x(x_r|x_s,\omega)$ points in the positive towline direction. The other possible outcome is when $E_x(x_r|x_s,\omega)$ points in the negative towline direction. The above derivation can be started with a requirement of a maximum in the inline electric field,

$$E_x(x_r|x_s,\omega) = e_x(x_r|x_s,\omega)\cos(\theta) - e_y(x_r|x_s,\omega)\sin(\theta). \quad (10)$$

This also results in equation 8, but with a sign reversal for the second derivative in equation 9. An alternative approach to finding the rotation angle can be based on the rotation ellipse as discussed by Smith and Ward (1974). However, this method does not resolve the problem of differentiating between the positive and negative inline directions. In order to discriminate between these two solutions, additional information must be used. This information can be retrieved from the data if the transmitter current data are analyzed in combination with the receiver data.

ABSOLUTE PHASE

A realistic analysis of the electromagnetic field close to an electric dipole in sea water, relevant for SBL data, must be performed with both an air layer above and a formation below the transmitter. This is the procedure followed when QC or correction tables used for processing are constructed. However, for pedagogical reasons we discuss the problem of a horizontal electric dipole in seawater whole-space first. For distances up to about one hundred meters from the transmitter this model is sufficiently realistic.

The derivation of the electric Green's tensor in a homogeneous medium is given in Ward and Hohmann (1987). Let ϵ_0 be the electric permittivity of a vacuum with ϵ the relative permittivity. The conductivity is σ. The complex electric permittivity is then,

$$\widetilde{\epsilon} = \epsilon\epsilon_0 + i\frac{\sigma}{\omega}. \quad (11)$$

With μ the magnetic permeability, the complex wavenumber is determined by,

$$k_\omega^2 = \mu\widetilde{\epsilon}\omega^2. \quad (12)$$

The distance R between the source position x_s and the observation position x is

$$R = |x - x_s|, \quad (13)$$

and the Green's function solving the Helmholtz equation is,

$$g_0(x|x_s) = \frac{e^{ik_\omega R}}{4\pi R}. \tag{14}$$

Using the auxiliary quantity $a(k_\omega R)$,

$$a(k_\omega R) = \frac{i}{k_\omega R} - \frac{1}{(k_\omega R)^2}, \tag{15}$$

the electric Green's tensor for an electric dipole source can be expressed,

$$G_{mn}^{EJ}(x|x_s) = i\omega\mu\Bigg\{(1 + a(k_\omega R))\delta_{mn} - (1 + 3a(k_\omega R))$$

$$\times\left(\frac{x_m x_n}{R^2}\right)\Bigg\}g_0(x|x_s), \tag{16}$$

such that the electric field is given by,

$$E_m(x) = \int dx_s G_{mn}^{EJ}(x|x_s)J_n(x_s). \tag{17}$$

The electric field due to a realistic, finite length, electric dipole source can be found by an integral over infinitesimal electric dipole source elements using equation 17. The magnetic Green's tensor for an electric dipole source is,

$$G_{mn}^{HJ}(x|x_s) = -ik_\omega\left(1 + \frac{i}{k_\omega R}\right)\epsilon_{mnl}\frac{x_l}{R}g_0(x|x_s), \tag{18}$$

where ϵ_{mnl} is the Levi-Civita tensor. The magnetic field due to a realistic, finite length, electric dipole source is given by,

$$H_m(x) = \int dx_s G_{mn}^{HJ}(x|x_s)J_n(x_s). \tag{19}$$

The above Green's tensors can be analyzed as functions of the ratio of distance R over skin depth δ. The skin depth is determined by frequency and conductivity,

$$\delta = \frac{\sqrt{2}}{|k_\omega|} = \frac{503}{\sqrt{f\sigma}}. \tag{20}$$

The analysis shows that the near-field contributions are potentially large for the electric field at distances less than one skin depth and may be of importance several skin depths away from the source. The near-field effects are much smaller for the magnetic field and the phase gradient is modified, compared to the far-field value, at distances of approximately one fifth of the skin depth or less.

RESULTS

The measured electric and magnetic data are normally transformed from the time domain to the frequency domain. A range of source receiver offsets can be specified. From the navigation we can find the time corresponding to each source receiver offset. The signal is then extracted for some periods around this time and the trace is transformed to the frequency domain. The actual number of periods will naturally depend on the base frequency of the survey. Simultaneously, traces with identical time intervals are extracted from the transmitter signal and transformed to the frequency domain. The electric and magnetic data are then normalized by the phase of the transmitter signal. This normalization can be achieved by multiplying the electric and magnetic data by the absolute value of the current divided by the complex number representing the current. The results are the electric fields measured in V/m and magnetic fields measured in A/m with absolute phase. Alternatively, the electric and magnetic data can be normalized with the dipole moment, which is the electric current (complex number) times the dipole length. This gives normalized electric fields measured in V/Am^2 and normalized magnetic fields measured in 1/m^2 with absolute phase.

A real dataset is displayed in Figure 1. The water depth at the receiver location is 2100 m. Figure 1a shows the amplitudes of the measured horizontal electric fields. The e_x component is in black and the e_y component is in red. The source receiver offsets are from -10 to 10 km. The data are not saturated at small and zero offset. This is an important property when the phase is calculated for these offsets. The amplitudes of the two components are of equal size. Thus, in this case the receiver has landed on the seabed with an orientation that is close to $\pm45°$ or $\pm135°$ relative to the towline. This is supported by the horizontal magnetic fields shown in Figure 1c. The h_x component is in black and the h_y component is in red. The amplitudes of the two components are of equal size. Figure 1b shows the phases of the horizontal electric fields. The e_x component is in black and the e_y component is in red. The two components are shifted 180° with respect to each other. A 180° phase shift (π in radians) is the same as a difference in sign,

$$e^{\pm i\pi} = -1. \tag{21}$$

The reason for the difference in sign is that one component is oriented in the positive towline direction and one component is oriented in the negative towline direction. If the receiver is oriented at $-45°$ or $+135°$, then both components should have the same sign. At $-45°$ orientation both e_x and e_y point in the positive towline direction. At

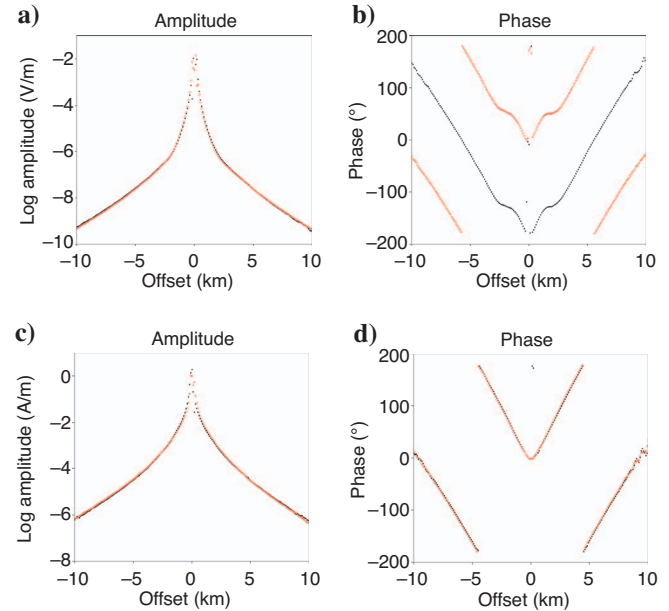
Figure 1. Field data prior to inline rotation. (a) Electric amplitude. (b) Electric phase. (c) Magnetic amplitude. (d) Magnetic phase. The electric x-component is black, the electric y-component is red, the magnetic x-component is black, and the magnetic y-component is red. The transmitter length is 270 m.

+135° orientation both e_x and e_y point in the negative towline direction. Thus, this receiver must point in either the +45° direction or in the −135° orientation. This can also be deduced directly from equation 2 with the crossline electric component, E_y, equal to zero,

$$e_x(x_r|x_s, \omega) = E_x(x_r|x_s, \omega)\cos(\theta),$$
$$e_y(x_r|x_s, \omega) = -E_x(x_r|x_s, \omega)\sin(\theta). \quad (22)$$

Equation 22 shows that if the rotation angle is +45° or −135°, the measured e_x and e_y components have opposite signs. For the magnetic field we can assume that H_x is small or negligible. The corresponding equations for the measured magnetic components are then,

$$h_x(x_r|x_s, \omega) = H_y(x_r|x_s, \omega)\sin(\theta),$$
$$h_y(x_r|x_s, \omega) = H_y(x_r|x_s, \omega)\cos(\theta). \quad (23)$$

Equation 23 indicates that if the rotation angle is +45° or −135°, the measured h_x and h_y components have the same sign. This is confirmed by Figure 1d which shows magnetic phase curves that lie on top of each other, indicating that they have the same sign.

Figure 2a shows the amplitudes of the horizontal electric fields after the inline rotation angle is found from equations 8 and 9 and the application of this angle in equation 1. The actual rotation angle in this case is +44° or alternatively −136°. Thus, after rotation, the E_x component in Figure 2a is oriented either 0° or ±180° with respect to the towline direction. Figure 2b shows the phase of the inline horizontal electric field, E_x. This curve can be used to resolve the 180° ambiguity; a method is proposed later in this section.

The E_y component is now close to two orders of magnitude smaller than the E_x component. The normal situation, when processing real data, is that we are left with an E_y component that differs from zero after inline rotation. There are several reasons for this. As previously mentioned, if there is transmitter-generated noise in the data, we cannot expect the E_y component to be zero, but it is a good approximation that it is minimum, given a plane layer geometry and a transmitter pointing in the towline direction. A different problem is that for a real earth the plane layer symmetry is always broken to some degree. Then there is the possibility that the E_y component is excited along the towline. The assumption of a minimum in E_y is still reasonable for situations with relatively small variations in geometry. An additional problem is that, because of seawater currents, the transmitter may not point directly in the towline direction. The implication is that there must be an E_y component that is different from zero also along the towline. Some of this effect may be minimized by the median filtering approach, but there remains the possibility that the seawater current is consistent over the whole towline. This situation can be detected since the transmitter direction is measured, but the correction is not always straightforward. If the deviation between the towline direction and the transmitter direction is less than approximately 10° it might still be reasonable to require a minimum in E_y as an optimization criterion. If this deviation is larger and the data are acquired in shallow water we have an additional problem even for plane layer geometry. There is a contribution from the airwave that modifies the polarization direction of the field along the towline direction if the transmitter is not pointing in the inline direction. It is clear that, because of the above-mentioned problems there are cases where the E_x component does not point in the exact towline direction but represents a maximum amplitude direction. The resulting data are still useful for further processing, but the interpretation of final results must be done bearing these inaccuracies in mind.

Figure 2c shows the amplitude of the horizontal magnetic fields after the inline rotation angle is found from the rotation equations for the magnetic field. These equations are similar to equations 8 and 9 for the electric field. The H_x component is now close to two orders of magnitude smaller than the H_y component. Figure 2d shows the phase of the crossline horizontal magnetic field H_y. Alternatively, this curve can be used to resolve the 180° ambiguity. The magnetic rotation angle differs less than 0.1° from the electric rotation angle for this data set. The rotation angles are shown in Figure 3 as a function of offset, prior to median filtering. The black marks are for the electric field and the red marks are for the magnetic field. The offsets are from 400 to 9700 m. Each subinterval where the weight differs from zero is 300 m. The first offset here is smaller than what is normally used in production. The electric and magnetic rotation angles are determined from median filtering these two sets.

The inline rotation procedure is normally based on intermediate and large offsets. Next we introduce two additional procedures that concentrate on the minimum source receiver separation. The first of these resolves the 180° ambiguity and the second is used to analyze timing errors. Timing errors are best analyzed at very small source receiver offsets because propagation effects are minimal when the source receiver separation is minimal. The measured phase is dominated by propagation through seawater and the disturbance from the formation is minimal.

The phase of the electric or magnetic field can be analyzed as a function of the distance between the source and the observation point. If the gradient of this function is small, the corresponding phase velocity must be large. The reason is, when the phase velocity is large, all the observation points will be at a similar phase. A well-
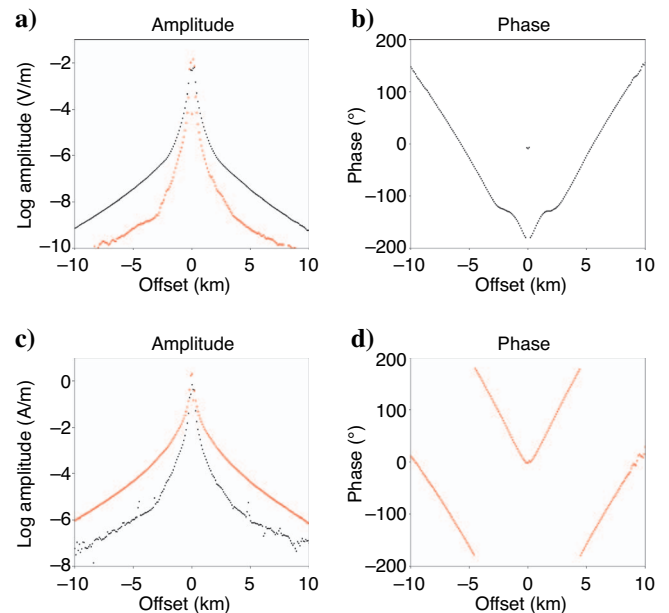

Figure 2. Field data after inline rotation. (a) Electric amplitude. (b) Electric phase. (c) Magnetic amplitude. (d) Magnetic phase. The electric x-component is black, the electric y-component is red, the magnetic x-component is black, and the magnetic y-component is red. The final determination of the direction of the inline electric component or the magnetic crossline component is not done at this stage. Two potential solutions exist. One where the inline electric component is in the positive towline direction and one where the electric inline component is in the negative towline direction.

known example is the airwave which has a large phase velocity. The phase curve plotted as a function of the source/receiver offset is nearly flat. In general the gradient becomes steeper with reduced phase velocity. Figure 4 shows the distribution of the phase of the inline electric field in the x-z plane. The source location is (0,0,0). The cross section is in the source plane. The x-axis is denoted distance and the z-axis is denoted depth. The frequency is 0.25 Hz and the conductivity is 3.33 S/m. These values give a plane-wave phase velocity of 866 m/s and a skin depth of 551 m. The inline electric field is given by equation 17, and is caused by an electric dipole of 270 m in length. Figure 5 is a trace in the depth direction from Figure 4 with an x-position of 0. Figure 6 is a trace in the x-direction from Figure 4 with a depth 10 m below the source location. The electric field shows strong near-field effects. This is apparent in Figure 5 where we see that the phase gradient is very small the first 500 m away from the source location. A small phase gradient indicates a large phase velocity in this area. The electric field appears nearly instanta-

neous here, even if we are in a strongly conductive medium. At larger offsets the gradient is increased and approaches a value corresponding to that of a plane wave with a phase velocity of 866 m/s. For a plane wave with this phase velocity, the phase will increase 104° over 1000 m.

Another interesting and important observation can be seen in Figure 6 (but is also apparent in Figures 4 and 5). The phase is not zero close to the source, but is close to 180°. If the transmitter is an infinitesimal horizontal electric dipole (very short HED), this phase equals 180° with a good approximation. In our case, we use an HED with a length of 270 m. The deviation from 180° is caused by the finite length of the transmitter dipole. The phase at zero offset (minimum source receiver separation) is 162° in the given example. At zero offset in Figure 6 the observation (receiver) location is 10 m below the midpoint of the transmitter. If the transmitter runs a current in the positive x-direction, then the return current in the seawater must be in the negative x-direction at this location. This is the reason for the close to 180° phase shift.

This is illustrated in Figure 7, where the source current is from left to right. The current immediately below the transmitter, at position P2, is pointing in the opposite direction. This is also the local direc-
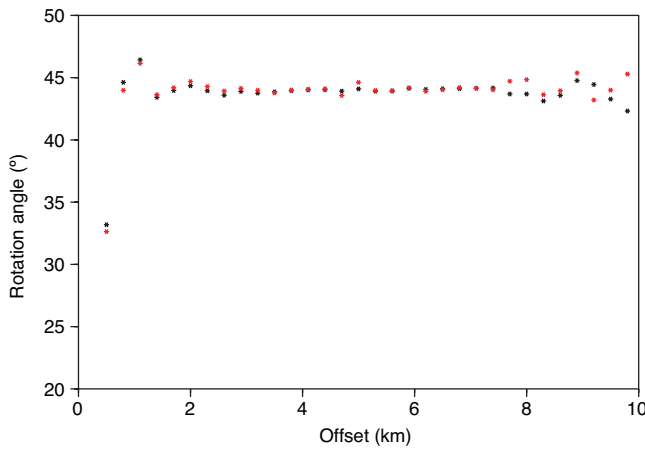

Figure 3. Rotation angles as a function of offset. The black marks are for the electric field and the red marks are for the magnetic field. The electric and magnetic rotation angles are determined from median filtering these two sets.
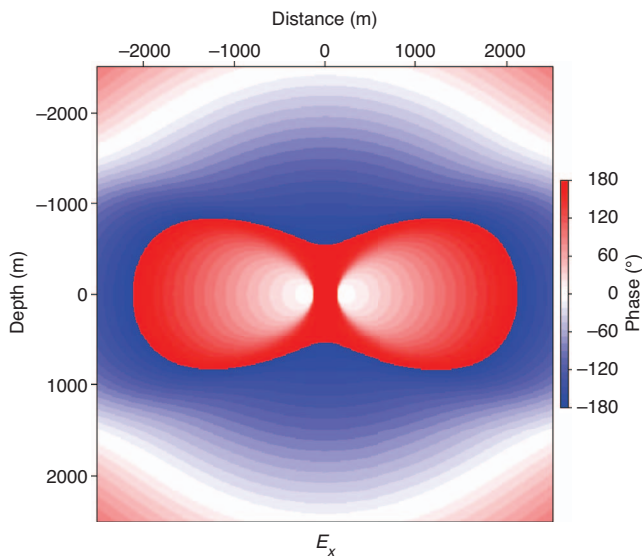

Figure 4. Distribution of phase for the electric inline field in an x-z cross section through the source plane.
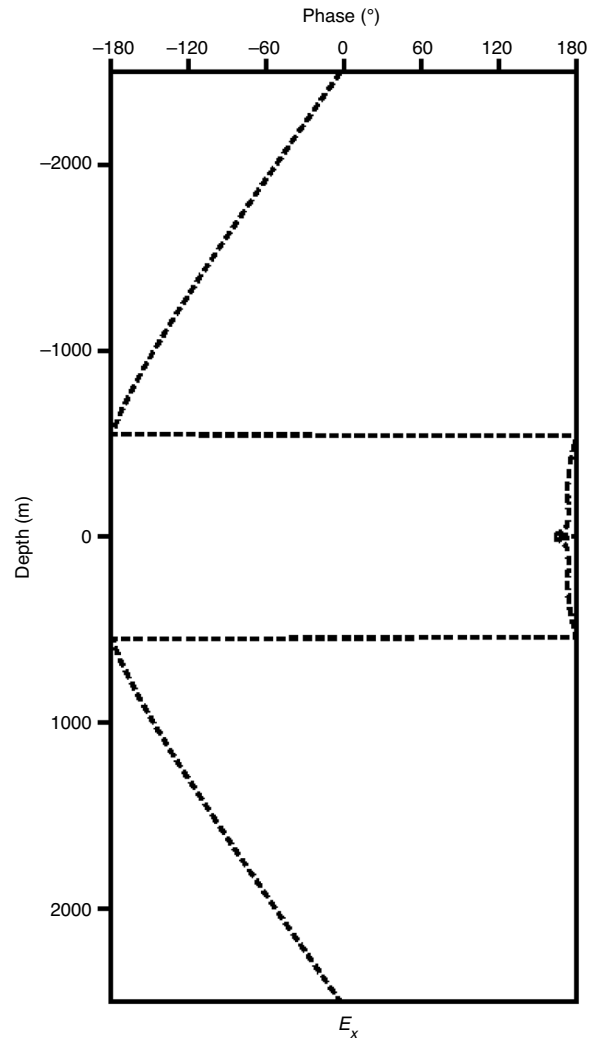

Figure 5. Distribution of phase for the electric inline field. This is a depth trace through the source location.

tion of the inline electric field. The inline electric field at position P2 is 180° out-of-phase with the source current since it is directed in the negative x-direction. If we move to a location immediately in front of the transmitter, at position P3 in Figure 7, or immediately behind the receiver, at position P1 in Figure 7, Figure 6 shows that the phase drops to slightly more than 0°. The inline electric field here is in phase with the source current. From Figure 7 we see that this is in accordance with the radiation pattern of an electric dipole in a conducting medium. The current, and hence the inline electric field, at these locations are in the positive x-direction as is the source current. For larger offsets the phase increases with distance.

The fact that the electric current in seawater immediately below the transmitter must be close to 180° out-of-phase with the transmitter can be used at the final stage of the receiver rotation procedure described previously. Going back to the inline electric field in Figure 2,
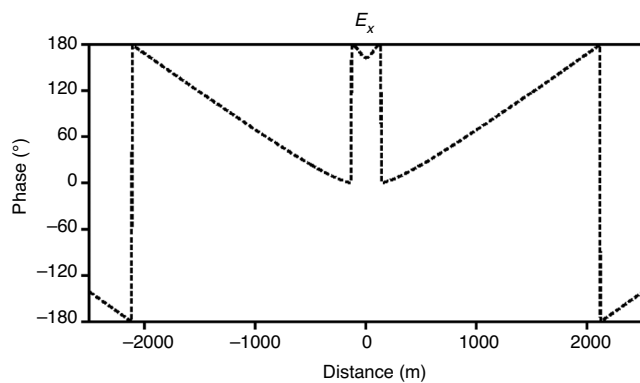

Figure 6. Distribution of phase for the electric inline field. Distance/offset trace recorded 10 m below the source depth.
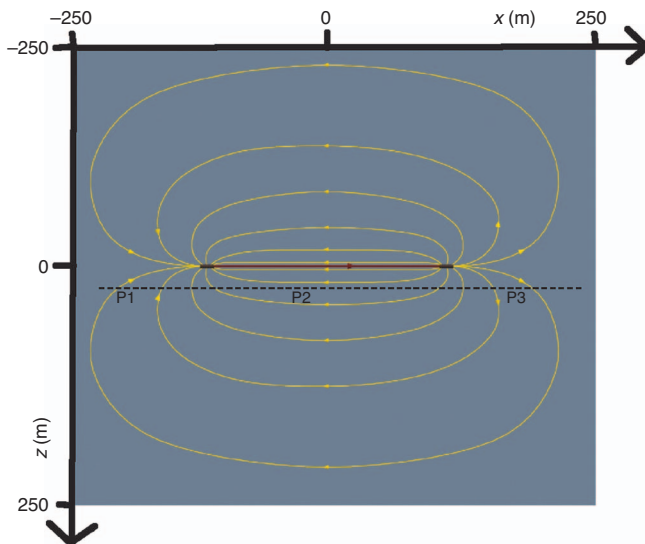

Figure 7. Radiation pattern for a horizontal electric dipole (HED). The source current of the HED is from left to right which is also the positive x-direction. The return current in seawater is marked as yellow lines. The direction is marked with arrows. This is also the direction of the electric field at the location. The inline electric field points in the direction of the source current at position P1 and position P3. The inline electric field points in the opposite direction of the source current at position P2. This amounts to a phase shift of close to 180 degrees of the electric field at P2 with respect to the source current.

we observe that the phase at zero offset does not compare well with the inline electric field in Figure 6 since it is shifted −180°. The receiver in Figure 2 is oriented in the negative inline direction. This can be corrected by multiplying the electric and magnetic fields, represented by complex numbers, by −1. This does not change the amplitude, but gives a 180° spatial rotation. The result is shown in Figure 8. The electric phase is shown in Figure 8b. The electric phase is now close to 180° at zero offset and drops to close to 0° in front of and behind the transmitter. The phase gradient at intermediate and large offsets is smaller in the real data in Figure 8b than in the synthetic data in Figure 6. The reason is that we have used a model with seawater only for the synthetic data. The real data is influenced by propagation of the electric field in a formation that has lower conductivity and hence higher propagation velocity than seawater. However, when source receiver separations are very small, the direct field in seawater dominates the response and the assumption of a close to 180° phase is still valid for zero or minimum offset. As a consequence of the final spatial rotation, the magnetic phase also changes 180° and is close to −180°. This can be seen in Figure 8d. The interpretation is that the magnetic field at the minimum offset and below the transmitter points in the negative y-direction in the inline coordinate system. This is in accordance with the right-hand rule.

A proper analysis of the electric near field for an SBL experiment requires that the effects of the formation and the air layer are included. In this case, analytical expressions are no longer available, but extensive modeling studies can be used to build up sufficient information. An example of the electric inline component, $E_x(x_r|x_s, \omega)$, for a realistic formation is shown in Figure 9. The transmitter length is 270 m. Three frequencies are shown for this case: 0.25 Hz (black), 0.75 Hz (red), and 1.25 Hz (blue). From Figure 9 it is clear that the zero offset inline electric phase is frequency dependent. The 0.25 Hz zero offset phase is 175°. The 0.75 Hz zero offset phase is 166°. The 1.25 Hz zero offset phase is 159°. For the above example the water depth is 500 m, the water resistivity is 0.27 Ωm and the top forma-
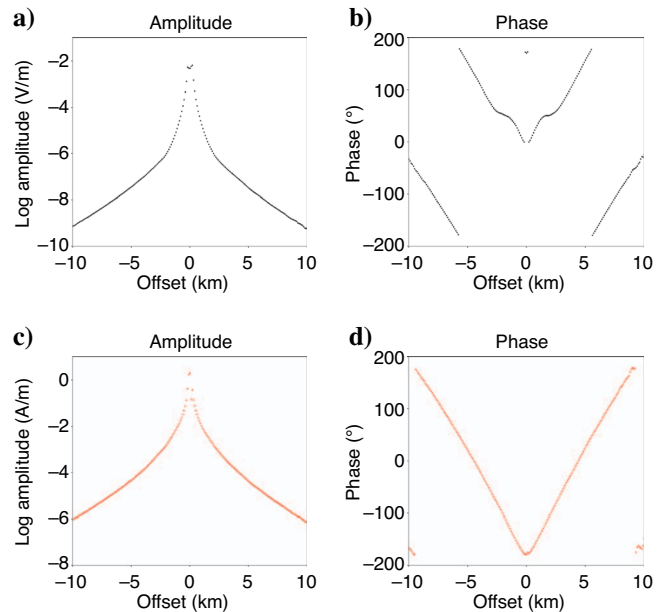

Figure 8. Field data after inline rotation and final 180° direction correction. (a) Inline electric amplitude. (b) Inline electric phase. (c) Crossline magnetic amplitude. (d) Crossline magnetic phase.

tion resistivity is 1 Ωm. There is also one deeper layer starting at 1 km below the seabed with resistivity 3 Ωm. The zero offset phases in Figure 9 are not very sensitive to water depth unless the water depths approach 100 m. In this case the zero offset phase at 0.25 Hz rotates forward 1° and the zero offset phase at 1.25 Hz rotates forward 3°. The corresponding phase rotations for 200 m water depth are 0.3° and 1°, respectively. Likewise, we observe some sensitivity to top formation resistivity as low as 0.5 Ωm, but find little variation if it varies between 1.0 and 4.0 Ωm.

We have experience with inversion of SBL data from many locations worldwide. Generally we need top formation resistivities between 1.0 and 3.0 Ωm to explain the data. If there are cases with lower resistivity in the top formation or with water depths on the order of 100 m, these cases require special attention. For the following analysis we concentrate on the most important parameters determining the zero offset phase. These are the transmitter length L the distance from the transmitter midpoint to the receiver R_0, the angular frequency ω, and the seawater conductivity σ_w. All these quantities are measured in an SBL survey. If the source is not towed directly above the receiver, a true horizontal zero offset cannot be realized. However, a minimum horizontal offset can still be found. The smallest R_0 value will be for this minimum horizontal offset. It is the total distance between the midpoint of the transmitter and the receiver that is most important for the phase properties. At these small distances ($R_0 \leq 100-200$ m) the direct radiated field is dominantly axially symmetric and it is not a requirement that the transmitter is towed directly above the receiver. The configuration we seek is similar to position P2 in Figure 7, but with the receiver possibly to one side of the transmitter.

The smallest transmitter/receiver distance can be obtained from navigation since the source elevation is measured. This configuration can also be identified directly from the data since there will be two 180° phase shifts in the electric field during transmitter passing. The first occurs when the front electrode passes the receiver and the

second occurs when the aft electrode passes the receiver. The data we need for the our analysis are midway between these two events. There are clearly navigation problems if the coordinates for this position do not coincide with the smallest source receiver distance. In the following we will refer to the minimum horizontal offset also as zero offset.

Synchronization

If the synchronization between transmitter clock and receiver clock is lost for some reason, then it may be possible to recover from this failure by closely inspecting the electric data at zero offset. The procedure requires a four-parameter table to be precalculated by forward modeling. This table must contain the absolute phase as a function of the transmitter length, the distance from transmitter midpoint to the receiver, the frequency, and the seawater conductivity. By comparing the zero offset phases for all frequencies of the inline real data with the tabulated value, a single, averaged, time delay or time advance $\Delta\tau$ can be deduced. Assume that the measured zero offset phase for the inline electric component is $\phi_{E_x}(\omega)$ and the tabulated inline zero offset phase is $\phi_{TAB}(\omega, L, R_0, \sigma_w)$. Then,

$$\omega\Delta\tau = \phi_{E_x}(\omega) - \phi_{TAB}(\omega, L, R_0, \sigma_w). \qquad (24)$$

If n_ω frequencies are available, one possible averaging procedure is,

$$\Delta\tau = \frac{1}{n_\omega}\sum_\omega \frac{\phi_{E_x}(\omega) - \phi_{TAB}(\omega, L, R_0, \sigma_w)}{\omega}. \qquad (25)$$

Figure 10 shows the phase of the crossline magnetic field, $H_y(x_r|x_s, \omega)$. The formation, frequencies, and transmitter length are the same as for the inline electric field in Figure 9. From Figure 10 it is clear that the zero-offset crossline magnetic phase is less frequency dependent than the zero offset inline electric phase. The 0.25 Hz zero offset phase is −179.5°. The 0.75 Hz zero offset phase is −178.8°. The 1.25 Hz zero offset phase is −178.1°. In general, the zero offset crossline magnetic phase shows much less variation with transmitter length, distance from the transmitter midpoint to the receiver, frequency, and seawater conductivity than the zero-offset electric phase. The zero-offset crossline magnetic phase is less sensitive to top formation conductivity and total water depth than the zero-offset inline electric phase. In general we find the effects on the zero-offset crossline magnetic phase to be less than 0.5 degrees. The largest effects on the zero-offset crossline magnetic phase can be observed when the frequency is above 1 Hz and the distance from the transmitter midpoint to the receiver is more than 100 m. In this case the zero-offset magnetic phase can be −170° to −160°. For frequencies less than 1 Hz and R_0 less than 100 m, the zero offset magnetic phase is usually between −180° and −175°.

The behavior of zero-offset electric and magnetic phases as a function of frequency and minimum distance is shown in Figure 11. The solid lines are for a minimum distance of 30 m and the dashed lines are for a minimum distance of 60 m. The electric phases start out at +180° and rotate as far back as +135° for the 30 m minimum distance and back to +150° for the 60-m minimum distance at 2 Hz. The magnetic phases start out at −180° and rotate forward to −177.5° for the 30 m minimum distance and forward to −173° for the 60-m minimum distance at 2 Hz. Figure 11 shows that the variation in phase with frequency and also minimum distance is much less for the magnetic field than for the electric field. Hence, the minimum distance magnetic phase is better suited for timing analysis than the
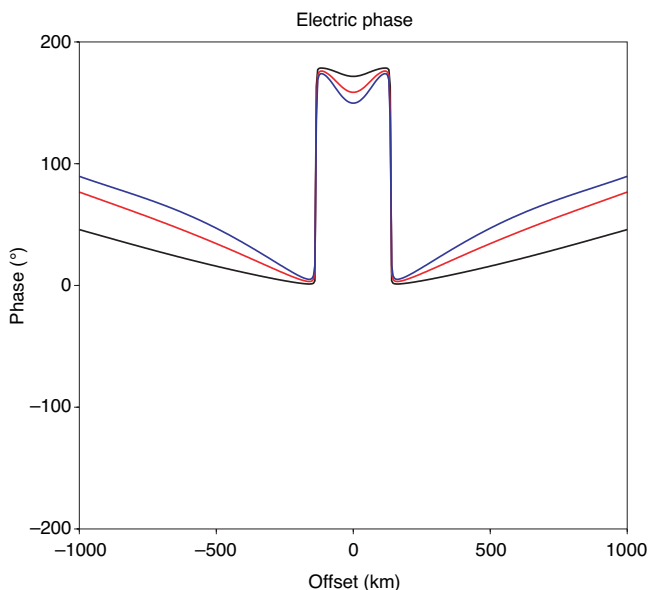

Figure 9. Modeled inline electric data from a 270 m long HED and $R_0 = 30$ m. The black line is 0.25 Hz, the red line is 0.75 Hz, and the blue line is 1.25 Hz. The figure represents a small subset of all simulations used to build the electric absolute phase correction tables.

corresponding electric phase, simply because nearfield effects are smaller, assuming a realistic electric dipole, and because the frequency dependence is smaller. In other words, at frequencies less
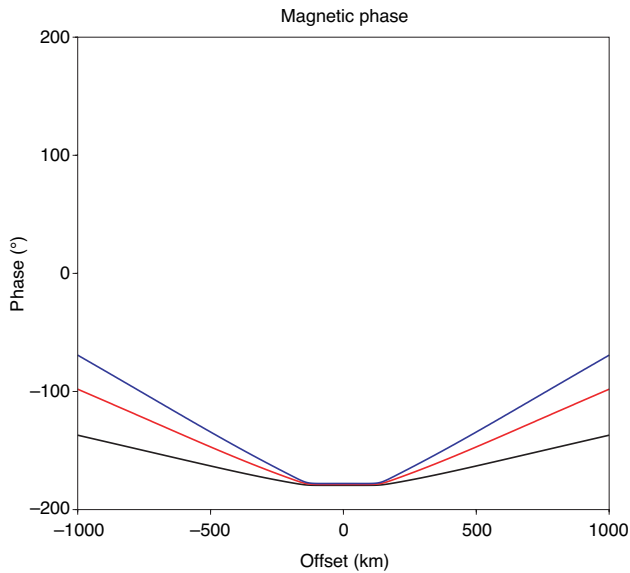

Figure 10. Modeled crossline magnetic data from a 270-m-long HED and $R_0 = 30$ m. The black line is 0.25 Hz, the red line is 0.75 Hz, and the blue line is 1.25 Hz. The figure represents a small subset of all simulations used to build the magnetic absolute phase correction tables.

than 1 Hz and for transmitter/receiver minimum distances less than 100 m, we know that we have a synchronization problem if the magnetic phase differs much from $-180°$.

Figure 12 shows phase as a function of distance for the electric and the magnetic fields. The upper curve is for the electric field and the lower curve is for the magnetic field. The frequency is 0.5 Hz. The magnetic phase changes by 4° over the first 100 m. The temporal sampling interval during data acquisition is normally 20 ms. At 0.5 Hz a synchronization error of 5 ms gives a phase error of approximately 1°. A navigation error of 25 m gives a similar phase error. The navigation accuracy for receiver position is less than 1% of the slant range and the accuracy for the transmitter position is better than 0.5%. Thus, the accuracy in source-receiver offset is within 25 m at 2000 m water depth or shallower.

The electric phase at the minimum distance R_0 depends on the transmitter length. We have already established that propagation increases the phase. Increasing the transmitter length has the opposite effect. The phase of the electric field at R_0 is decreased. Apparently the electric field arrives earlier than expected, but this cannot be a noncausal effect. Figure 13 shows the electric field, the magnetic field, and the transmitter current in the time domain for $R_0 = 30$ m and for a transmitter length equal to 270 m. The period is 4 s. The fields are calculated with a plane layer algorithm. Both the electric and the magnetic fields are close to $\pm180°$ out-of-phase with the transmitter current. Thus, the transmitter current is multiplied by -1 before plotting in Figure 13. The electric field is in black, the magnetic field is in red, and the transmitter current is in blue. All amplitudes are normalized such that the plateau levels are equal to ±1.
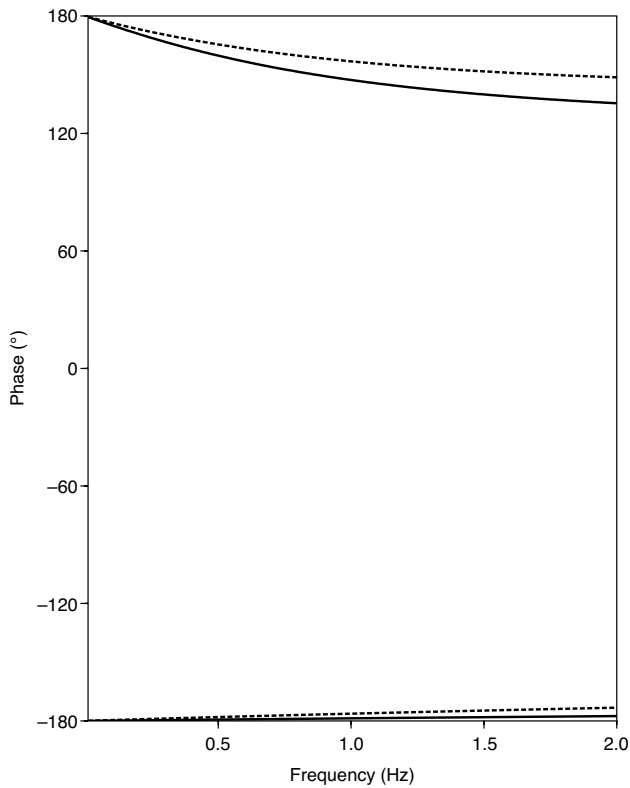

Figure 11. Electric and magnetic phases as a function of frequency at minimum offset. The two lower curves are for the magnetic field. The two upper curves are for the electric field. The solid lines are for $R_0 = 30$ m and the two dashed lines are for $R_0 = 60$ m.
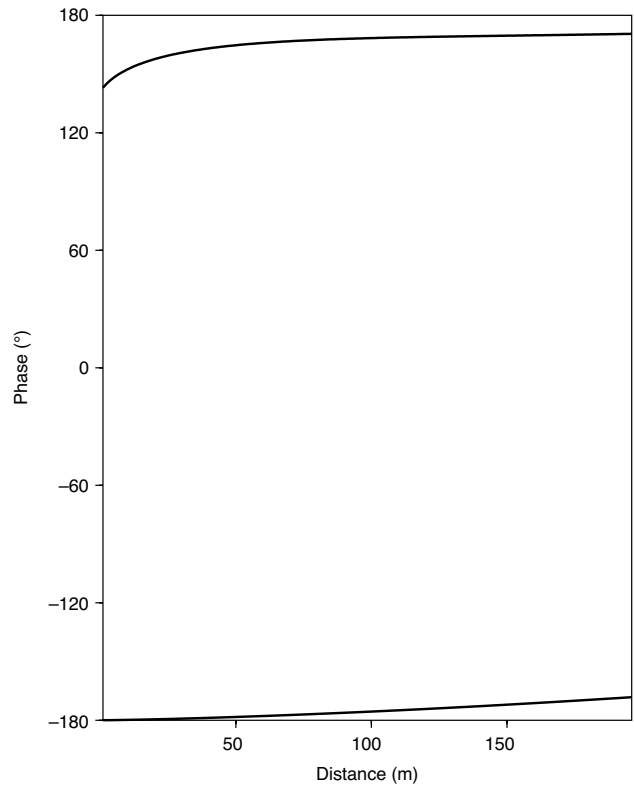

Figure 12. Phase as a function of distance for the electric and the magnetic fields. The upper curve is for the electric field and the lower curve is for the magnetic field.
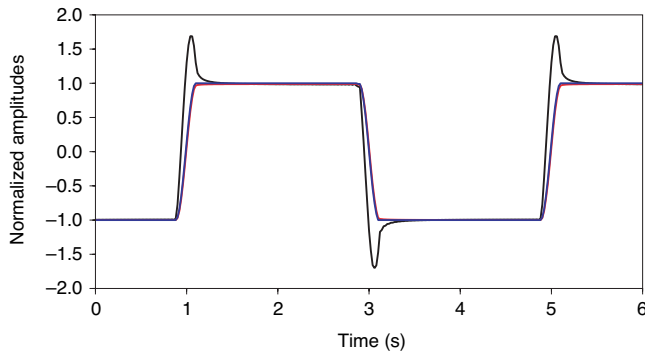
Figure 13. Synthetic data. Time domain response of the electric and magnetic phases at minimum offset. The electric field is black, the magnetic field is red, the negative of the transmitter current is blue. All amplitudes are normalized such that the plateau levels are equal to ±1.
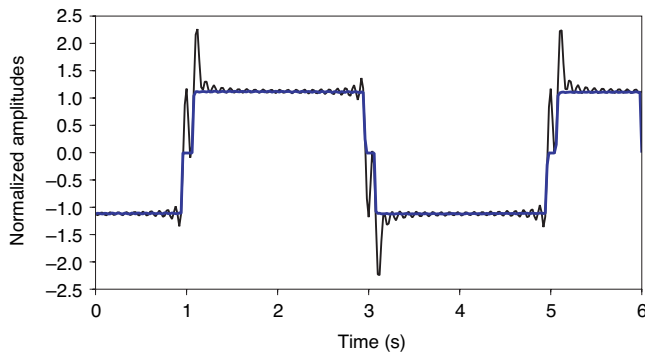

Figure 14. Real data. Time domain response of electric phase at minimum offset. The electric field is black and the negative of the transmitter current is blue. The amplitudes are normalized such that the plateau levels are equal to ±1.

With the given normalization, we observe that the magnetic field follows the transmitter current closely. This is not so for the electric field. We see an overshoot of the electric field following the switching of the transmitter current. However, it is clear that the electric field has a causal behavior. There are no changes in the electric field before the current is switched, but the rise time is shorter for the electric field than for the transmitter current and the magnetic field. The phases are mainly determined by the zero crossing of the traces. The electric field trace has an earlier zero crossing than the transmitter current. Accordingly, the electric phase is rotated backward when normalized with the transmitter phase in the frequency domain.

A thyristor-based transmitter cannot switch instantaneously between positive and negative current directions when the current is 1000 A. It will have a switching interval of approximately 80–100 ms where the current is zero. The result is that there will be two overshoot effects in the electric field at R_0. The first is when the current is switched off and the second is when the current is switched on with the opposite polarity. This will influence the phase of the measured electric field. A real data example is shown in Figure 14. In order to determine the absolute phase at R_0, we need receivers that do not saturate at small offsets. If the receiver saturates at small offsets, one possible effect is that only the first overshoot with corresponding

zero crossing is picked up. This will give a timing error of at least 50 ms. In the frequency domain and at 0.25 Hz this will rotate the phase of the electric field at least 5° backward.

CONCLUSIONS

A receiver dropped onto the seabed will end up with an arbitrary orientation, which means that the recorded electric and magnetic x- and y-components will point in arbitrary directions. Both electric and magnetic data can be used to rotate the field data to a coordinate system where the x-direction points in the inline or towline direction or 180° with respect to this direction. The amplitudes of electric and magnetic marine CSEM data are strongly offset dependent so we introduce an offset dependent weighting function to equalize the contributions from different offsets. We tried several weighting schemes for the inline rotation procedure. Presently, we use a median filtering approach that handles the strong offset dependence and is also reasonably robust with respect to noise.

An inspection of electric and/or magnetic phase after normalization with the source-current phase can resolve the remaining problem of the 180° spatial rotation. The final result is electric and magnetic data where the x-component points in the positive towline direction.

In the case of lost temporal synchronization between the receivers and the transmitter, the proper absolute phase can be recovered approximately by introducing precalculated tables for zero offset electric and/or magnetic phases. These tables depend on the frequency, the transmitter length, the distance between the receiver and the midpoint of the transmitter, and the water conductivity. These four quantities are measured during a marine CSEM survey. The method requires electric and/or magnetic data that are not saturated at short offsets.

The magnetic zero offset phase shows less variation with these four parameters than the electric zero offset phase. Hence, if magnetic data are available, they are preferable to electric data for this type of processing.

ACKNOWLEDGMENTS

REFERENCES

Constable, S., 1990, Marine electromagnetic induction studies: Surveys in Geophysics, **11**, 303–327.
Constable, S., and C. Cox, 1996, Marine controlled source electromagnetic sounding 2: The PEGASUS experiment: Journal of Geophysical Research, **101**, 5519–5530.
Cox, C., J. Filloux, and J. Larsen, 1971, Electromagnetic studies of ocean currents and electrical conductivity below the ocean floor, *in* A. Maxwell, ed., The sea: John Wiley & Sons, Inc., 637–693.
Eidesmo, T., S. Ellingsrud, L. M. MacGregor, S. Constable, M. C. Sinha, S. Johansen, F. N. Kong, and H. Westerdahl, 2002, Sea bed logging (SBL), a new method for remote and direct identification of hydrocarbon filled layers in deep-water areas: First Break, 20, 144–152.
Ellingsrud, S., T. Eidesmo, M. C. Sinha, L. M. MacGregor, and S. Constable, 2002, Remote sensing of hydrocarbon layers by seabed logging (SBL): Results from a cruise offshore Angola: The Leading Edge, **21**, 972–982.
Key, K., 2003, Application of broadband marine magnetotelluric exploration to a 3D salt structure and a fast-spreading ridge: Ph.D. dissertation, U.C. San Diego, 40–42.
MacGregor, L., M. Sinha, and S. Constable, 2001, Electrical resistivity structure of the Valu Fa Ridge, Lau Basin, from marine controlled-source elec-

tromagnetic sounding: Geophysical Journal International, **146**, 217–236.

Mittet, R., L. Løseth, and S. Ellingsrud, 2004, Inversion of SBL data acquired in shallow waters: 66th Annual Conference and Exhibition, EAGE.

Smith, B. D., and S. H. Ward, 1974, On the computation of polarization ellipse parameters: Geophysics, **39**, 867–869.

Ward, S. H., and G. W. Hohmann, 1987, Electromagnetic theory for geophysical applications, *in* M. N. Nabighian, ed., Electromagnetic methods in applied geophysics — Theory: SEG, 131–311.

Young, P., and C. Cox, 1981, Electromagnetic active source sounding near the East Pacific Rise: Geophysical Research Letters, **8**, 1043–1046.

Yuan, J., and R. N. Edwards, 2000, The assessment of marine gas hydrates through electrical remote sounding: Hydrate without a BSR?: Geophysical Research Letters, **27**, 2397–2400.